Eur Biophys J (2012) 41:79–87
DOI 10.1007/s00249-011-0761-9

ORIGINAL PAPER

EBSA
Biophysics in Europe

Depth-sensing analysis of cytoskeleton organization based on AFM data

Katarzyna Pogoda · Justyna Jaczewska · Joanna Wiltowska-Zuber · Olesya Klymenko · Kazimierz Zuber · Maria Fornal · Małgorzata Lekka

Received: 10 July 2011 / Revised: 30 September 2011 / Accepted: 11 October 2011 / Published online: 27 October 2011

Abstract Atomic force microscopy is a common technique used to determine the elastic properties of living cells. It furnishes the relative Young's modulus, which is typically determined for indentation depths within the range 300–500 nm. Here, we present the results of depth-sensing analysis of the mechanical properties of living fibroblasts measured under physiological conditions. Distributions of the Young's moduli were obtained for all studied cells and for every cell. The results show that for small indentation depths, histograms of the relative values of the Young's modulus described the regions rich in the network of actin filaments. For large indentation depths, the overall stiffness of a whole cell was obtained, which was accompanied by a decrease of the modulus value. In conclusion, the results enable us to describe the non-homogeneity of the cell cytoskeleton, particularly, its contribution linked to actin filaments located beneath the cell membrane. Preliminary results showing a potential application to improve the detection of cancerous cells, have been presented for melanoma cell lines.

K. Pogoda · J. Jaczewska · J. Wiltowska-Zuber · O. Klymenko · K. Zuber · M. Lekka (✉)
The Henryk Niewodniczański Institute of Nuclear Physics, Polish Academy of Sciences, Radzikowskiego 152, 31-342 Kraków, Poland
e-mail: Malgorzata.Lekka@ifj.edu.pl

J. Jaczewska
The Smoluchowski Institute of Physics, Jagiellonian University, Reymonta 4, 30-059 Kraków, Poland

M. Fornal
The Department of Internal Medicine and Gerontology, Collegium Medicum, Jagiellonian University, Śniadeckich 10, Kraków, Poland

Keywords Cell biomechanics · Atomic force microscopy · Depth-sensing analysis · Cell cytoskeleton

Abbreviations

AFM	Atomic force microscopy
MEM	Minimum essential medium
EDTA	Ethylenediaminetetraacetic acid
PBS	Phosphate-buffered saline
FWHH	Full width of the distribution taken at half height

Introduction

Mechanical forces are important in the regulation of a variety of biological processes at the molecular and cellular levels, for example gene expression, adhesion, or migration, that are essential to the maintenance of tissue homeostasis (Zhu et al. 2000; Liu et al. 2009; DeMali et al. 2003). It has been reported that eukaryotic cells respond to external mechanical stimuli by adjusting their biochemical and biomechanical properties (Lekka et al. 1999, 2001; Schrot et al. 2005; Pesen and Hoh 2005). Therefore, thorough understanding of cell mechanics is important to advances in cell biology, medicine, and tissue engineering.

The development of such techniques as atomic force microscopy (AFM; Seo and Jhe 2008) has enabled biomechanical measurements at the single cell level, very frequently under liquid conditions imitating the natural environment. The AFM measurement is accomplished by indenting the cell by using a cantilever (i.e. a delicate spring) as a probe, and by recording its deflection during the process. By comparing the deflections, recorded on a stiff surface (usually a glass coverslip on which cells are

cultured) and on a cell, *force versus indentation curves* can be obtained. This relationship is a basis for determination of the relative Young's modulus of the cell. Its value, describing cell stiffness, is a very local feature which is usually used for comparison of the elastic properties of the cell, for example to distinguish cancerous cells (Lekka et al. 1999). Such studies have clearly shown much smaller Young's modulus (i.e. larger deformability) for cancerous bladder cells ($\sim$1 kPa) than for reference cells ($\sim$10 kPa). Similar results were obtained when other reference and cancerous cells were investigated (Guck et al. 2005; Remmerbach et al. 2009; Li et al. 2008).

The contribution of structural components of the cell cytoskeleton to AFM-determined mechanical properties has been discussed in several studies. These have demonstrated the importance of both structural and cytoskeleton-associated proteins. Such measurements were performed for different cells types. Complete and comparative studies of cytoskeleton integrity have been already presented by Wu et al. (1998) and Rotsch and Radmacher (2000). The results have shown that actin filaments are mostly responsible for the mechanical properties of cells, because disruption of the microtubules had no effect when measured using AFM. Another reason for this is that the magnitude of the indentation depth is usually chosen to be less than 500 nm.

In our work, we present the results of depth-sensing studies of the mechanical properties of living cells (fibroblasts, cancerous melanoma cells, and erythrocytes) measured under physiological conditions. Fibroblasts represented cells with a highly organized internal structure. The results were compared with two other samples with simpler and relatively homogenous cell interior, i.e. erythrocytes and fibroblasts with depolymerized actin filaments. The relative Young's modulus, determined for indentation depths ranging from 200 to 1400 nm, revealed a depth-dependent relationship attributed to differences between the interior organization of the cells. Comparison between these two limits showed that for small indentation depth ($\sim$200 nm) heterogeneity of the distribution of actin filaments was observed whereas for large indentations (1400 nm) an averaging effect was present. On the basis of these results, comparison of two melanoma cell lines, i.e. from a primary cancer site (WM35) and from a highly metastatic site (A375), was performed to show the potential use of the proposed analysis to improve the detection of cancerous cells.

Materials and methods

Cell lines

Healthy human fibroblasts (human skin fibroblasts CCL110; LGC Promochem) were grown in Eagle's medium (MEM; Sigma-Aldrich) supplemented with 5% fetal calf serum, 1% penicillin and streptomycin, and 1% L-glutamine. Two human cell lines, WM35 (primary cutaneous melanoma cell line from the radial growth phase) and A375 (a metastatic melanoma cell line), were grown in culture medium RPMI 1640 (pH 7.4) containing 10% fetal calf serum.

All cells were cultured in plastic Petri dishes then trypsinized using trypsin–EDTA solution (0.05%; Sigma) and spread on glass coverslips (Knittel, 15 mm $\times$ 15 mm). Cells were kept at 37°C in an atmosphere of 95% air/5% CO_2 and high humidity (>98%). They were taken for AFM measurements 3–5 days later.

Cytochalasin D

Cytochalasin D (Sigma) was dissolved in 10 mM phosphate-buffered saline (PBS, MP Biomedicals, pH 7.4, containing 150 mM NaCl, 27 mM KCl, Sigma) at a final concentration of 5 μg/ml. Fibroblasts were cultured on glass coverslips as for AFM measurements. After 2–3 days, they were washed with PBS and incubated with cytochalasin D for 10 min in the incubator. After incubation cells were washed with PBS and immediately measured by AFM in MEM buffer.

Erythrocytes deposition

Glass coverslips (Menzel-Gläser, 22 $\times$ 22 mm^2) were cleaned with acetone then immersed in 0.01% w/v poly-L-lysine solution (Sigma) for 5 min. This increased the number of amino groups causing better adhesion of cells to the glass substrate. The glass coverslips were then dried in a clean atmosphere for 24 h at room temperature.

A drop ($\sim$200 μl) of heparinized blood was deposited on a pretreated glass coverslip and incubated for 45 min at room temperature. The coverslip was then washed with PBS to remove unbound or loosely bound erythrocytes. Such prepared samples of blood cells were immediately measured by AFM in PBS.

Fluorescence microscopy

Cells, cultured on glass coverslips (Marienfeld; radius 25 mm), were washed with PBS, and a 2% solution of paraformaldehyde (Fluka) was added for 30 min to fix them. After removing the fixative, cells were incubated with a 0.2% solution of Triton X-100 at 4°C for 5 min, followed by rinsing with PBS. The coverslips were then incubated with Alexa-Fluor 488 conjugated with phalloidin (1:100; PBS solution; Molecular Probes) for 30 min, washed again with PBS, and closed.

All fluorescence measurements were performed using an Olympus IX71 microscope equipped with a 100-W

mercury lamp (uniformly illuminating the whole sample area), and a U-MWIG2 filter ($\lambda_{exit} = 530–550$ nm, $\lambda_{emit} > 580$ nm), and an objective (UPlanApo) at magnification 600×. For image recording, an XC10 digital camera was used. This camera provides a 1,376 × 1,032 pixel (1.4 million) image with a 2/3 in. optical format. Images were recorded using the program Cell A.

Atomic force microscopy

Measurements of cell elastic properties were performed using a home-built device described elsewhere (Lekka et al. 1999), which for the same cantilever type enables recording of large indentation depths up to 2000 nm. The cell topography was recorded by use of a commercial microscope (model XE-120; Park Systems). To control the position of the AFM tip and to locate a cell, an optical microscope was used.

In our studies, two types of silicon nitride cantilever, MLCT-AUHW and MSNL (Veeco), were used as probes. Both types of cantilever were characterized by a spring constant of 0.01 N/m. Fibroblasts and melanoma cells were measured with the MLCT-AUHW cantilever, and erythrocytes with the MSNL type. The shape of the AFM tip is a four-sided pyramid with height varying from 2.5 to 8 μm. Both tip types have a small radius of curvature (2 and 50 nm for MNSL and MLCT, respectively) compared with the size of indentations used in our studies (from 200 to 1400 nm). Thus, independently of the cantilever type used, penetration of the AFM tip into the cell never exceeded half of its height (Fig. 1a). The typical cell height was in the range 3.0–3.5 μm.

Before the measurement, each coverslip with cells was washed three times with PBS. Fibroblasts were measured in MEM buffer, melanoma cells in RPMI buffer, and erythrocytes in PBS. All measurements were performed at room temperature.

Data acquisition

Force curves were collected from randomly chosen cells (a fibroblast, a melanoma cancerous cell, or an erythrocyte) located by use of an optical microscope only. No imaging was performed before elasticity measurements. The scan size was then set to a square of 12.6 × 12.6 μm^2 (256 × 256 pixels). On each chosen region (around the cell center) a grid of 12 × 12 points (with a distance between points of 49.2 nm) was created. On average, 144 curves for each single cell were automatically saved. The loading force was set in such a manner that the maximum indentation depth reached 1400 nm, i.e. between 3 and 4 nN. Above this value, the effect of a hard substrate was observed.

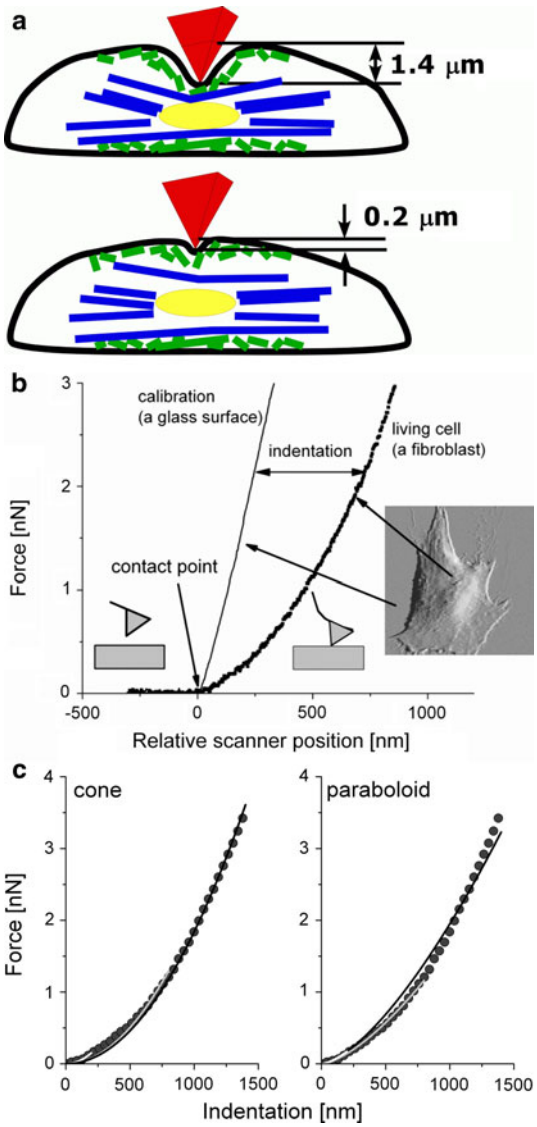

Fig. 1 **a** Depth-sensing analysis furnishes information about the heterogeneity of the structure of the cell interior. **b** The Young's modulus is determined by subtraction of curves recorded on hard (in our case glass coverslip) and soft (fibroblasts) surfaces. **c** Comparison between fits obtained for models assuming either parabolic or conical shape of the AFM tip (*lines* correspond to the fit performed for indentations of 200, 800, and 1400 nm; *black points* are experimental data)

Cell topography was recorded at a scan rate between 1.0 and 1.5 Hz and a set point in the range 0.3–0.5 nN. Scan size of 70 × 70 μm (256 × 256 pixels) was chosen to visualize whole fibroblasts whereas their fragments were recorded as images of 30 × 30 μm^2 (256 × 256 pixels).

Cell stiffness

Cell stiffness is determined on the basis of the *force versus indentation curve* that is usually obtained by subtraction of cantilever deflections measured on stiff and compliant surfaces at a given, relative sample position (Fig. 1b).

When a stiff material (not easily deformable, for example silicon or glass) is investigated, the deflection reflects the position of the sample. This is represented by a straight sloped line which is usually used as a reference line that is needed for the force calibration. For compliant samples, for example cells, cantilever deflections are much smaller and the resulting force curve is non-linear in character. The difference between these curves determines the deformation of the sample surface. Depending on the magnitude of the indentation depth, distinct properties can be studied, revealing the heterogeneity of the structure of the cell interior (Fig. 1a).

The *force versus indentation* curve describes the mechanical response to the applied load, which is characteristic for each material. The relative Young's modulus value, characterizing the cell stiffness, can be evaluated in the framework of Hertz contact mechanics, taking into account an infinitely stiff indenter with a selected geometry of the AFM tip (i.e. spherical, parabolic, conical, or flat-ended) and a flat, deformable substrate (Sneddon 1965). Usually, the AFM probe tip is a four-sided pyramid that can be modeled either by a cone or by parabola. Thus, two formula are usually used to describe the relationship between the loading force and the resulting indentation depth:

- for a conical tip:

$$F(\delta) = \frac{2}{\pi \cdot \tan(\alpha)} \cdot E_{\text{eff}} \cdot \delta^2 \tag{1}$$

- and for a parabolic tip:

$$F(\delta) = \frac{4}{3} \cdot \sqrt{R} \cdot E_{\text{eff}} \cdot \delta^{\frac{3}{2}} \tag{2}$$

where F is the loading force, α the open angle (35° and 22.5° for MLCT and MNSL cantilevers, respectively), R the radius of curvature of the AFM tip, E_{eff} the reduced Young's modulus, and δ the indentation depth. The reduced Young's modulus is given by:

$$\frac{1}{E_{\text{eff}}} = \left(\frac{1 - \mu_{\text{tip}}^2}{E_{\text{tip}}} + \frac{1 - \mu_{\text{sample}}^2}{E_{\text{sample}}} \right). \tag{3}$$

When $E_{\text{sample}} \ll E_{\text{tip}}$ (as is true for living cells) then:

$$E_{\text{eff}} = \frac{E_{\text{sample}}}{1 - \mu_{\text{sample}}^2} \tag{4}$$

where μ_{sample} and μ_{tip} are the Poisson ratios, related to the compressibility of the sample material, ranging from 0 to 0.5. The Poisson ratio for cells is difficult to determine, therefore, all calculations must assume its value. Very often this value is set to be equal 0.5, because cells can be treated as the incompressible material. The final Young's modulus of a cell was calculated taking into account all values determined for the whole set of *force versus indentation curves* recorded for a single cell.

The force–indentation curves, obtained for all studied cell types, were analyzed assuming that the shape of the AFM probe is a cone. The choice of the model was dictated by chi-squared values describing the goodness of the fit. They were smaller for the model with a conically shaped AFM tip than when a parabolic shape was assumed (Fig. 1c). The figure presents the idea of the Young's modulus determination at different indentation depths. After choosing the contact point position, the fit was performed at different indentation depths (lines denote the corresponding fit).

Results

Actin filaments organization

Actin filaments are the first cytoskeletal structures indented by the AFM tip. They are composed of G-actin subunits forming a thin, polar thread with diameter of approximately 7 nm. The G-actin subunits can be added to both (+) and (−) ends, but it is known that elongation of the (+) end is faster. The whole structure is highly dynamic and exists as a continuous balance between actin monomers polymerization and depolymerization. Although actin filaments are dispersed throughout the entire cell, they are concentrated mainly in the cortex layer beneath the plasma membrane. Therefore, our studies began with examination of the organization of actin filaments in fibroblasts. This was achieved by use of both atomic force and fluorescent microscopes. The images of surface topography showed actin filaments lying beneath the cell membrane (Fig. 2). They are organized into two groups:

1 stress fibers visible at lower magnifications (larger scans); and
2 short actin filaments.

The organization of actin filaments, constituting the cell cytoskeleton, was also observed by use of a fluorescent microscope. Actin filaments were stained using Alexa-Fluor 488 phalloidin of F-actin. Similarly to the AFM images, the stress fibers were also visible (Fig. 3a) in living fibroblasts.

The organization of actin filaments was disturbed after incubation for 10 min at 37°C with the actin-destabilizing agent cytochalasin D (5 μg/ml) (Fig. 3b). Stress fibers disaggregate after such treatment, and this was manifested in the lack of the long and thick structures observed for untreated cells. Moreover, because phalloidin binds to

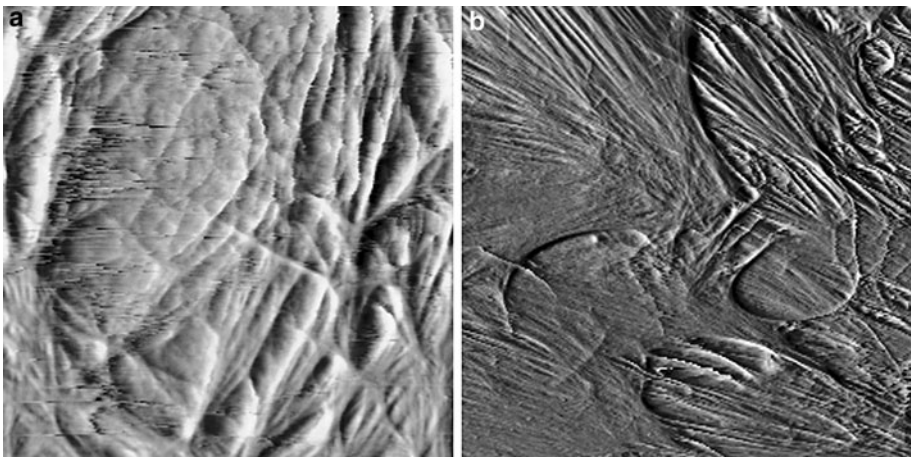

Fig. 2 Typical surface topography ("error mode") of the fibroblasts recorded for: **a** a scan size of 70 × 70 μm^2 and the set point at 0.33 nN; **b** a scan size of 30 × 30 μm^2 and the set point at 0.5 nN

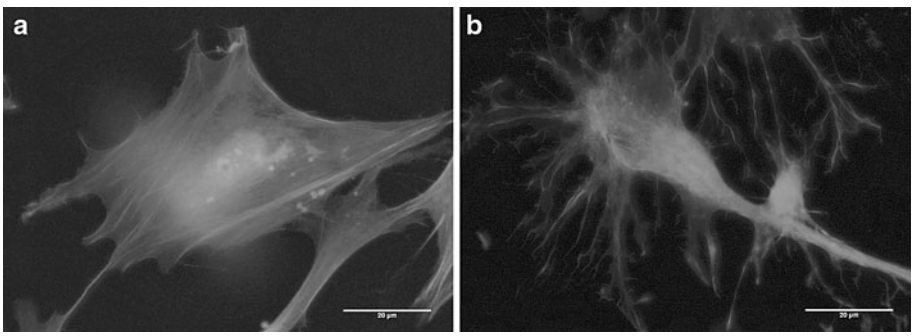

Fig. 3 Fluorescence images of the actin cytoskeleton of fibroblasts before (**a**) and after (**b**) treatment with cytochalasin D (5 μg/ml for 10 min at 37°C, magnification ×600)

F-actin and not to G-actin, the fluorescence image obtained indicates that stress fibers were cut into short filaments.

Fibroblasts stiffness

Taking into account the heterogeneity of the fibroblasts structure, the elastic properties were analyzed using both constant and variable values of the indentation depths. Three types of sample (living fibroblasts, fibroblasts treated with cytochalasin D, and erythrocytes, each possessing distinct organization of cytoskeleton) were analyzed.

Constant indentation depth

In our studies, the relative Young's modulus was calculated for two constant indentation depths, 200 and 1400 nm, because these are border limits in the presented depth-dependent analysis. Figure 4 shows histograms with distinct character of the Young's modulus distribution, depending on the chosen indentation depths. At small indentations the histograms created were wide, irrespective of the chosen individual cell. The widest distribution was obtained for living fibroblasts ($n = 132$ force curves) where the width of the distribution was above 2.5 kPa (taken as the full width taken at half height, FWHH, Fig. 4a). The fibroblasts treated with cytochalasin D ($n = 56$ force curves) and erythrocytes ($n = 134$ force curves) furnished histograms almost half as wide as that for living cells (FWHH = 1.5 kPa, and FWHH = 1.4 kPa, respectively).

At indentation depth equal to 1400 nm, the Young's modulus histograms showed much narrower distributions for all samples with FWHH within the range of 0.6–0.8 kPa (Fig. 4b; $n = 98$, 55, and 118 force curves were analyzed for fibroblasts, fibroblasts treated with cytochalasin D, and erythrocytes, respectively).

The effect was observed for all studied cells as it is presented in the distributions created for cell populations, taking into account all measured fibroblasts (Fig. 4c, 50 fibroblasts, 9 fibroblasts treated with cytochalasin D, and 12 erythrocytes were analyzed).

Similarly, the histograms obtained for a whole population of fibroblasts treated with cytochalasin D, and of erythrocytes were narrower. Also, at large indentations, the distribution of the Young's modulus for all cell populations were again narrower than those obtained for small indentations (Fig. 4d).

Furthermore, the increase of the indentation depth lowered the mean of the modulus irrespective of the

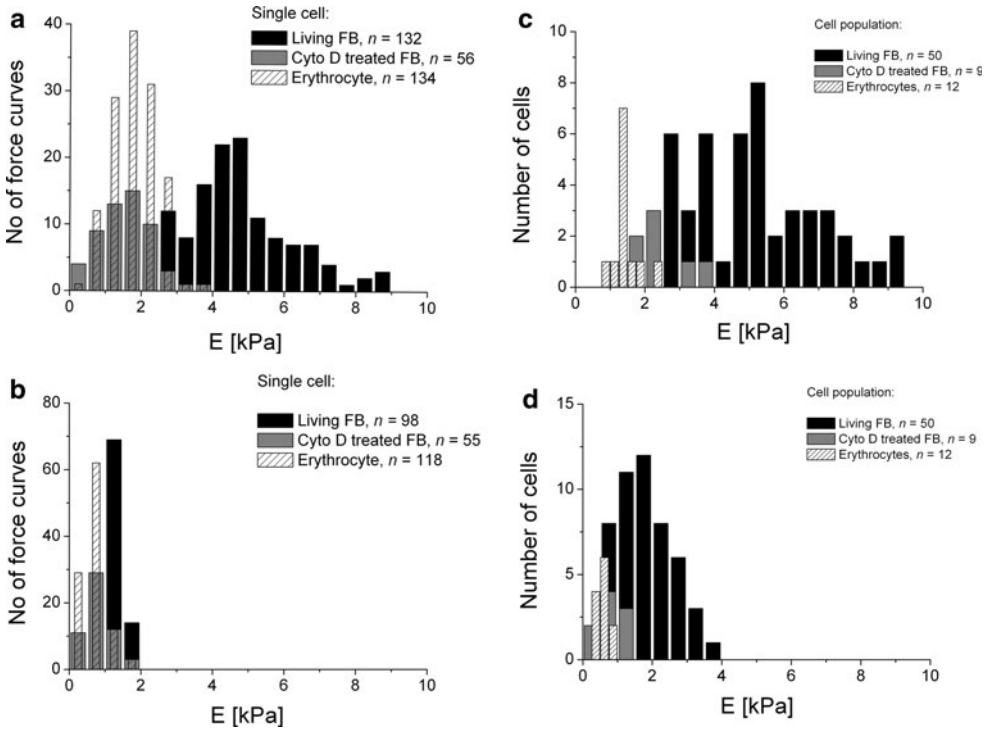

Fig. 4 Histograms of the relative values of the Young's modulus obtained for living fibroblasts (*black columns*), fibroblasts treated with cytochalasin D (*grey columns*), and erythrocytes (*white-spare columns*). Typical modulus distributions of a single cell obtained for indentation depths: 200 nm (**a**) and 1400 nm (**b**). Distributions for cell populations obtained analogously (**c**, **d** for 200 and 1400 nm, respectively). The force versus indentation curves were fitted assuming that the AFM tip can be represented as a cone. Bin size = 0.5 kPa, *n* denotes either the number of force curves or cells taken for the analysis

measured sample type. The most significant drop was observed for living fibroblasts whereas for cells treated with cytochalasin D and erythrocytes the Young's modulus dropped by a factor of 2 (Table 1).

Variable indentation depth

In our analysis, the data were calculated assuming the conical shape of the probing AFM tip. Figure 5a shows a randomly chosen single representative of all sample types (living fibroblasts, cytochalasin D-treated cells, and erythrocytes), where the Young's modulus was normalized for indentation equal to 200 nm (i.e. the corresponding Young's moduli were divided by the modulus value calculated for indentation equal to 200 nm).

This was done to obtain a value, independent of the initial Young's modulus, that was different both for each cell and for each location on a same cell (Lekka and Laidler 2009). The relationship between Young's modulus and indentation depth decreased most for living fibroblasts (black dots) whereas the weakest relationship was obtained for fibroblasts treated with cytochalasin D (stars). Erythrocytes were placed between them (black squares).

Then, the ratio R between the modulus values was calculated for the two limits of indentation depth 200 nm and 1200 nm. The R was introduced to quantify the observed effect (and to characterize the extent of disruption of actin filaments). Its value quantifies the degree of change as a function of indentation depth in relation to that obtained for 200 nm. Next, the Gauss function was fitted to each histogram of R-values, corresponding to the studied cell types, to obtain the center position of the distribution (Fig. 5b, lines not shown). The mean values ± standard deviations for all analyzed cell types are presented in Fig. 5c. Depending on the cell type, erythrocytes and fibroblasts, two distinct values of R are observed, as was confirmed by Student's t-test. Treatment of the fibroblasts with the cytochalasin D resulted in a slight increase of R accompanied by a large standard deviation, indicating large diversity in the elastic properties of a cell. Student's t-test

Table 1 Young's modulus for living fibroblasts, fibroblasts treated with cytochalasin D, and erythrocytes, all determined for 200 and 1400 nm indentation depths

Sample	E_{200} (indentation depth = 200 nm) (kPa)	E_{1400} (indentation = 1400 nm) (kPa)
Living fibroblasts ($n = 50$)	4.85 ± 2.03	1.66 ± 0.86
Fibroblasts treated with cytochalasin D ($n = 9$)	2.48 ± 1.49	0.83 ± 0.45
Erythrocytes ($n = 12$)	1.38 ± 0.12	0.57 ± 0.19

All values are presented as mean ± standard deviation (n denotes the number of measured cells)

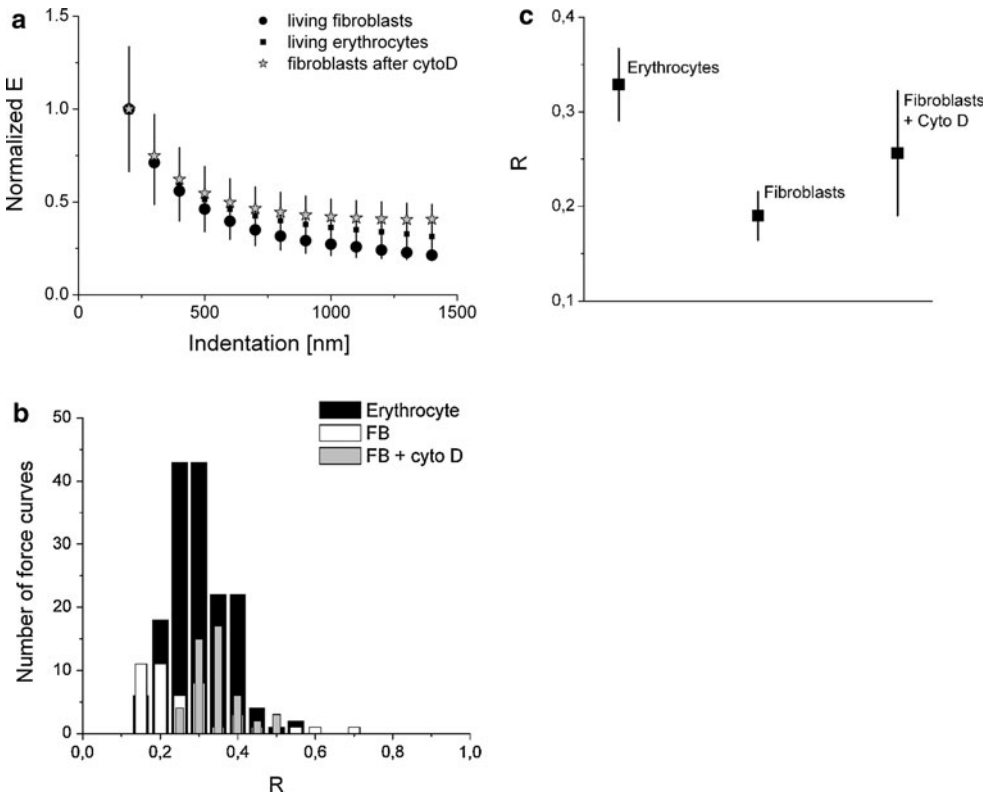

Fig. 5 **a** Typical dependence of the relative Young's modulus as a function of the indentation depth determined for living fibroblasts (*black dots*), erythrocytes (*black squares*), and fibroblasts treated with cytochalasin D (*stars*). **b** Distributions of R (defined as the ratio of E_{1200} to E_{200}) obtained for erythrocytes (*black columns*), living fibroblasts (*white columns*), and fibroblasts treated with cytochalasin D (*grey columns*). **c** Mean values of R determined for given cell sample types. *Errors* are standard deviations

showed a non-significant difference between cytochalasin D-treated fibroblasts and two other cell populations (at the $P = 0.05$ level). This can be explained by the different rate of the actin depolymerization process induced by cytochalasin D. Large variations indicate that cytochalasin D acts in both a depth and location-dependent fashion. At the same level ($P = 0.05$), the difference between the erythrocytes and fibroblasts was significant, showing that R can be used to distinguish between cell types.

Depth-sensing analysis for cancerous cells

Correct choice of indentation depth can be essential for such AFM applications as identification of pathologically changed cells occurring, for example, in cases of cancer. The proposed depth-sensing analysis was performed for two human melanomas: WM35 (primary cutaneous melanoma cell line from the radial growth phase) and A375 (metastatic melanoma) cell lines. The main difference between these cell lines is that WM35 cells are non-metastatic whereas A375 cells are highly invasive. Therefore, distinct organization of cell cytoskeleton was expected (Yamaguchi and Condeelis 2007). A representative relationship between Young's modulus and indentation depth is presented in Fig. 6.

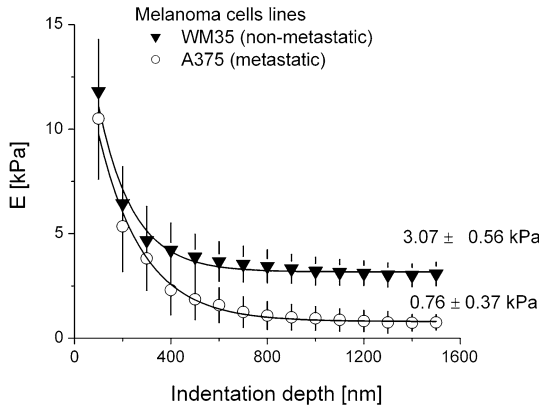

Fig. 6 Typical dependence of the relative Young's modulus as a function of the indentation depth determined for two melanoma cell lines: WM35 (non-metastatic cancer cells from a primary tumor site) and A375 (highly metastatic cells). Each *data point* represents a mean calculated for a whole cell (i.e. from ~140 locations recorded on a single cell). *Error bars* denote standard deviations

The cone approximation of the AFM tip was used to fit the data. However, the analysis was performed for these cells only, for which the fit using the parabolic approximation showed the sample-induced effect. The results clearly show that identification of cancerous cells on the

basis of elastic properties is possible for indentations larger than 500 nm.

Discussion

Many previous studies have shown that mechanical properties reflect the organization of the cell cytoskeleton (Canadas et al. 2002; Discher et al. 2009; Suresh 2007). The magnitude of its alteration can be described quantitatively by using the relative value of the Young's modulus, which can be obtained from AFM elasticity measurements. In such experiments, the modulus is calculated for indentation depths set within the range 300–500 nm (Li et al. 2008; Cross et al. 2008; Cuerrier et al. 2009).

When a constant indentation depth is chosen for the analysis, one can assume that the mechanical response comes from the same layer of the studied material. Thus, the direct comparison of different samples is fully justified (Lekka et al. 1999). Actually, the mechanical properties of a cell's surface are different from those of deeper parts of a cell. Small indentation depths essentially point to the region rich in actin filaments. The choice of larger values probes cell regions rich in two remaining cytoskeleton elements (i.e. microtubules and intermediate filaments). Thus, by use of such complementary measurements, the overall stiffness of the whole cell can be obtained.

Our main finding was that the elasticity moduli calculated for large indentation depths became smaller, accompanied by narrow distributions, whereas for small indentations depths the distribution was much broader. This could be explained by the fact that for small depths structures formed by actin filaments (short filaments and stress fibers) dominate in the determined stiffness. Thus, the heterogeneity of the stiffness distributions reveals the distinct and irregular organization of actin filaments lying beneath the cell membrane within a range of indentation up to 200 nm. To determine whether larger Young's modulus distribution observed for small indentation depths can be correlated with significant differences in cytoskeleton organization, we used fluorescence and atomic force microscopes to explore the cytoskeleton arrangements in the studied samples. On the basis of these images we observed different features of actin organization, which confirms the results obtained from AFM measurements.

Moreover, treatment of the cells with cytochalasin D, a cytoskeletal agent with the ability to bind to actin filaments and block their polymerization (Haidle and Myers 2004), resulted in changes in actin cytoskeleton morphology. As has been shown in a few earlier AFM experiments (Wakatsuki et al. 2001; Weichsel et al. 2010) cytochalasin D treatment results in loss of actin filaments that dramatically affects the cell's mechanical stability, reflected as a lower Young's modulus. The smaller number of stress fibers present in cells treated with cytochalasin D can explain why such cells are softer than untreated, living fibroblasts.

Another important finding is that the mechanical response of fibroblasts treated with cytochalasin D is not homogenous; this is reflected as a large width in the histogram of *R*. Disruption of the actin filaments should lead to more homogenous distribution of the cell cytoskeleton as in the case of erythrocytes, which can be approximated by a 2D bilayer—a cytoskeleton viscoelastic membrane that encloses homogeneous hemoglobin (Safran et al. 2005). Therefore, narrow histograms obtained for erythrocytes are not surprising and these cells can be used as a reference.

Application of the depth-sensing analysis to two melanoma cell lines revealed potential for improved detection of metastatic cells. The preliminary results presented showed it was possible to distinguish between non-malignant and metastatic cells by use of indentation depths greater than $\sim$500 nm. This is probably connected with cancer-related changes observed already in two other structural components of the cell cytoskeleton, i.e. microtubules and intermediate filaments (Zhou and Giannakakou 2005). Lack of a significant difference observed for smaller indentation depths (less than 500 nm) can be explained either by similar organization of actin filaments in both melanomas or remodeling induced by the extracellular matrix strongly affecting cell rigidity (Goetz et al. 2011).

Conclusions

The heterogeneous structure inside cells was a driving force for studies of their elastic properties as a function of indentation depths. The most important findings were a decrease of the Young's modulus as indentation depth increases, irrespective of the cell type studied (fibroblast, melanoma cells, and erythrocytes). Smaller modulus values were accompanied by reduction of the distribution width. The observed heterogeneity in Young's modulus present at small indentations depths can be interpreted on the basis of several phenomena including non-homogenous distribution of cytoskeleton density, remodeling of actin organization induced by extracellular matrix, removal of a limited number of filaments composing the network, or even disruption of cytoskeletal filaments induced by AFM indentations. In this region, very local AFM measurements of the cell's mechanical properties detect small/minute changes in the organization of the actin network. Narrower distributions obtained for large indentation depths show the overall Young's modulus reflecting the mechanical resistance of a whole cell.

The proposed approach of data analysis will enable consideration of the cell as a complex multilayered

structure, rather than a homogenous object, a clear distinction between superficial and deeper effects is possible, thus giving valuable indications about the components of the cytoskeleton, as affected by the action of a chemical, mechanical, or any physiological process.

The potential usefulness of the proposed analysis was demonstrated for melanoma cells, which were distinguished on the basis of mechanical properties determined for larger indentations.

Acknowledgments This work was partially supported by the project SMW (Single Molecule Workstation), grant agreement number 213717 (NMP4-SE-2008-213717), and by the projects of the Polish Ministry of Science and Higher Education numbers: N-N202-285738 (O.K.) and N-N402-47133 (M.F.).

References

Canadas P, Laurent V, Oddou C, Isabey D, Wendling S (2002) A cellular tensegrity model to analyse the structural viscoelasticity of the cytoskeleton. J Theor Biol 218:155–173

Cross SE, Jin YS, Tondre J, Wong R, Rao J, Gimzewski JK (2008) AFM-based analysis of human metastatic cancer cells. Nanotechnology 19:384003

Cuerrier CM, Gagner A, Lebel R, Gobeil F, Grandbois M (2009) Effect of thrombin and bradykinin on endothelial cell mechanical properties monitored through membrane deformation. J Mol Recognit 22:389–396

DeMali KA, Wennerberg K, Burridge K (2003) Integrin signaling to the actin cytoskeleton. Curr Opin Cell Biol 15:572–582

Discher D, Dong C, Fredberg JJ, Guilak F, Ingber D, Janmey P, Kamm RD, Schmid-Schoenbein GW, Weinbaum S (2009) Biomechanics: cell research and applications for the next decade. Ann Biomed Eng 37:847–859

Goetz JG, Minguet S, Navarro-Lerida I, Lazcano JJ, Samaniego R, Calvo E, Tello M, Osteo-Ibanez T, Pellinen T, Echarri A, Cerezo A, Klein-Szanto AJP, Garcia R, Kelly PJ, Sanchez-Mateo P, Cukierman E, Del Pozo MA (2011) Biomechanical remodelling of the microenvironment by stromal caveolin-1 favors tumor invasion and metastasis. Cell 146:148–163

Guck J, Schinkinger S, Lincoln B, Wottawah F, Ebert S, Romeyke M, Lenz D, Erickson HM, Ananthakrishnan R, Mitchell D, Käs J, Ulvick S, Bilby S (2005) Optical deformability as an inherent cell marker for testing malignant transformation and metastatic competence. Biophys J 88:3689–3698

Haidle AM, Myers AG (2004) An enantioselective, modular, and general route to the cytochalasins: synthesis of L-696, 474 and cytochalasin B. Proc Natl Acad Sci 101:12048–12053

Lekka M, Laidler P (2009) Applicability of AFM in cancer detection. Nat Nanotech (correspondence) 4:72

Lekka M, Laidler P, Gil D, Lekki J, Stachura Z, Hrynkiewicz AZ (1999) Elasticity of normal and cancerous human bladder cells studied by scanning force microscopy. Eur Biophys J 28:312–316

Lekka M, Laidler P, Ignacak J, Łabędź M, Lekki J, Struszczyk H, Stachura Z, Hrynkiewicz AZ (2001) The effect of chitosan on stiffness and glycolytic activity of human bladder cells. Biochim Biophys Acta 1540:127–136

Li QS, Lee GYH, Ong CN, Lim CT (2008) AFM indentation study of breast cancer cells. Biochem Biophys Res Commun 374:609–613

Liu W, Fan Y, Deng X, Guan Z, Li N (2009) Adhesion behaviors of human trophoblast cells by contact with endothelial cells. Colloid Surf B 71:208–213

Pesen D, Hoh HJ (2005) Micromechanical architecture of the endothelial cell cortex. Biophys J 88:670–679

Remmerbach TW, Wottawah F, Dietrich J, Lincoln B, Wittekind C, Guck J (2009) Oral cancer diagnosis by mechanical phenotyping. Cancer Res 69:1728–1732

Rotsch C, Radmacher M (2000) Drug-induced changes of cytoskeletal structure and mechanics in fibroblasts: an atomic force microscopy study. Biophys J 78:520–535

Safran S, Gov N, Nicolas A, Schwarz U, Tlusty T (2005) Physics of cell elasticity, shape and adhesion. Phys A 352:171–201

Schrot S, Weidenfeller C, Schaffer TE, Robenek H, Galla HJ (2005) Influence of hydrocortisone on the mechanical properties of the cerebral endothelium in vitro. Biophys J 89:3904–3910

Seo Y, Jhe W (2008) Atomic force microscopy and spectroscopy. Rep Prog Phys 71:016101

Sneddon IA (1965) The relation between load and penetration in the axisymmetric Boussinesq problem for a punch of arbitrary profile. Int J Eng Sci 3:47–57

Suresh S (2007) Biomechanics and biophysics of cancer cells. Acta Biomater 3:413–438

Wakatsuki T, Schwab B, Thompson N, Elson E (2001) Effects of cytochalasin D and latrunculin B on mechanical properties of cells. J Cell Sci 114:1025–1036

Weichsel J, Herold N, Lehmann MJ, Kraeusslich HG, Schwarz US (2010) A quantitative measure for alterations in the actin cytoskeleton investigated with automated high-throughput microscopy. Cytometry A 77:52–63

Wu WH, Kuhn T, Moy VT (1998) Mechanical properties of L929 cells measured by atomic force microscopy: effects of anticytoskeletal drugs and membrane crosslinking. Scanning 20:389–397

Yamaguchi H, Condeelis J (2007) Regulation of the actin cytoskeleton in cancer cell migration and invasion. Biochim Biophys Acta 1773:642–652

Zhou J, Giannakakou P (2005) Targeting microtubules for cancer chemotherapy. Curr Med Chem 5:65–71

Zhu C, Bao G, Wang N (2000) Cell mechanics: mechanical response, cell adhesion, and molecular deformation. Annu Rev Biomed Eng 2:189–226